Instantaneous Flow Analysis of Contractile Cytoskeletal Structures Affected by the Dysregulation of Kinesin and Tropomyosin Motors

Alexandre Matov[1, 2, 3, †], Andrea Bacconi[4, 5], and Jesse C. Gatlin[6]

[1] Department of Medicine, Weill Medical College of Cornell University, New York, NY 10021

[2] University of Information Science and Technology St Paul the Apostle, Ohrid, Macedonia

[3] Present address: DataSet Analysis LLC, 155 Jackson St, San Francisco, CA 94111

[4] Department of Cell Biology, The Scripps Research Institute, La Jolla, CA 92037

[5] Present address: 1859 Inc., 11425 Sorrento Valley Rd, San Diego, CA 92121

[6] Department of Molecular Biology, University of Wyoming, Laramie, WY 82071

[†] Corresponding author:

email: matov@datasetanalysis.com

Running Title: Analysis of Contractile Cytoskeletal Structures: Instantaneous Flow Tracking Applied to Microtubule and Filamentous Actin Dynamics

Key words: Contractile Cytoskeletal Structures, Mitotic Spindle, Actin Meshworks, Growth Cones, Monastrol, S-trityl-L-cysteine, Blebbistatin, Tropomyosin Isoforms, Weak Actin Binders, Instantaneous Flow Tracking Algorithm

COVER LETTER

This manuscript explores, for the first time, in a quantitative way, the changes occurring in epithelial cells after upregulation of a stronger and a weaker isoform of the actin binding protein tropomyosin. The main cytoskeletal proteins, actin and tubulin, regulate cellular homeostasis in normal physiology and in disease. As such, the modulation of actin and microtubule (MT) contractility and dynamics could deliver significant clinical results in the treatment of cancers and neurodegenerative diseases.

This hypothesis, regarding drug selection, I conceived and formulated in 2004 based on the effects of paclitaxel on the mitotic spindle (in data from Lisa Cameron of UNC). The manuscript focuses on the instantaneous flow analysis of contractile cytoskeletal structures affected by the dysregulation of kinesin and tropomyosin motors. My hypothesis is that mutations in cancer-causing genes can be linked to a particular set of deviations in MT and actin regulation and dynamics. Every aspect of tubulin dynamicity in living cells is controlled by multiple genes, whose up- or down-regulation is linked to resistance to therapy. About 70 MT-associated proteins and 80 proteins within the kinetochore complex can be targeted in RNA therapy. Each MT dynamics parameter exhibits a multi-modal distribution resulting from the contributions of four or five genes that regulate a particular aspect of MT homeostasis in each cell. Therefore, candidate drug regimens can be tested ex vivo for their ability to revert the concrete defects, neutralize the disrupting impact of the disease, and sensitize it to a therapy regimen with low toxicity.

I also hypothesize that we can (i) identify an ultimate responder per each molecular subtype (i.e., a regimen resulting in a complete response) and (ii) sensitize every tumor to one of the ultimate response regimens by modulating the cytoskeleton. This hypothesis I further formulated based on my computational work and analysis results in renal cell carcinoma. I discovered that a correlation exists between specific disease-associated point mutations in the VHL gene and particular patterns of MT dynamics. My work demonstrated that it is possible to associate dysregulation of specific aspects of MT

regulation to point mutations occurring within a particular domain of pVHL. Mutations in the MT-interacting/HIF1α-interacting domain appeared to be more often linked to changes in polymerization/depolymerization rates. In contrast, VHL mutations in the Elongin C interacting domain were more frequently associated with changes in the catastrophe and rescue frequencies. Dysfunctional pVHL tumor suppressor leads to pathogenesis as well as drug resistance in disease. Thus, the MT transcriptome can offer personalized biomarkers for early detection and targets to sensitize resistant disease.

Further, I evaluated the effects of six MT targeting drugs on the signatures in a panel of four breast cancer cell lines, which demonstrated an approach to optimize chemotherapy, and axonal degeneration in a mouse model to elucidate the neuroprotective cellular effects of NAD+. Fluorescent speckle microscopy (FSM) is a high-resolution microscopy technique for visualization of polymer flux in sub-cellular structures, such as the mitotic spindle, discovered in the late 90s in the laboratory of Ted Salmon at UNC. I contributed to the quantification of the complex low signal-to-noise ratio FSM image data. My focus was the development of novel computational algorithms for the detection and analysis of the so-called speckles, which form within the filamentous actin meshwork. In addition, I contributed to the development of computer vision tools for the analysis of fluorescently labeled focal adhesions and lipid rafts dynamics.

The Instantaneous Flow Tracking Algorithm is a specialized computer vision tool for the motion tracking of dense anti-parallel and fast-evolving flows of fiduciary markers, termed speckles. I developed this algorithm initially for measurements in mitosis and the analysis of the spindle organization. Cell division is one of the most critical and fundamental processes in life, but because it involves complicated macromolecular assemblies comprised of dynamic polymers (i.e., MTs), it is a process that is difficult to study. Small phenotypic changes are difficult to distinguish without the aid of computational tools. For this reason, I applied some of the tools I have developed to measure anti-parallel MT flows during cell division and to investigate the mechanisms by which the minus-end

directed motor protein, cytoplasmic dynein, and the oncoprotein 18, stathmin 1, contribute to the spindle organization. I have extended the utility of this software by adding numerical algorithms for robust detection of distinctive image keypoints and the analysis of interlinked molecular structures, such as the endoplasmic reticulum, and a plethora of features, such as lysosomes, not just actin and MT speckles.

I have developed a software suite (DataSet Tracker™) for real-time analysis designed to run on PCs, smartphones, and smart glasses hardware and suitable for resource-constrained, on-the-fly computing in microscopes without internet connectivity; a demo is available for viewing at datasetanalysis.com. My objective is to present the community with an integrated, easy to use by all, tool for resolving the complex dynamics of the cytoskeletal meshworks, intracytoplasmic membranous networks, and vesicle trafficking. It is my goal to have this integrated tool approved for use in the clinical practice.

The potential clinical application of the analytics approach outlined in this manuscript pertains to analyzing drug resistance in cancer therapy and the treatment of neurodegeneration. Cell therapy is becoming the forefront of precision medicine, and it would be critical to be able to anticipate the mechanisms of action of the engineered immune cells. Natural killer cells and cytotoxic T cells employ different mechanisms to kill their targets, for instance by secreting cytotoxic lysosomes using the MT cytoskeleton for trafficking and release. There is also a plethora of effects induced in the target cells, most well studied of which lead to apoptosis and ferroptosis, a recently identified potent, caspase-independent, mechanism of programmed cell death. The exact pathways activated during therapy can only be pinpointed by measuring its effects on the target proteins in patient-derived living cells. It is conceivable that for different patients, with overall very similar genetic profiles, a distinct type of engineered immune cells would be required. Given the availability of high-quality fundamental research equipment for high resolution live-cell microscopy in most university hospitals, what I propose is to embed in these systems real-time software for automated quantification and statistical analysis of

intracellular behavior. Introducing this quantitative imaging approach to the clinic would allow physicians to fine-tune, with a high level of certainty, the correct treatment regimen for each patient.

The main discoveries presented in the manuscript, based on published and newly generated imaging data, are related to the ability of the cell to adapt to a wide range of biochemical and mechanical perturbations. I have investigated this in the context of the two main cytoskeletal proteins, tubulin and actin. Tubulin has been the target of numerous therapeutic approaches for six decades now. Most of these therapies have been, in essence, a “black box” approach, where a treatment with debilitating side effects is administered, without having the ability to anticipate whether it would affect the desired target. In this manuscript, a quantitative evaluation of some of the more difficult to interpret effects of tubulin-targeting compounds has been reported together with an attempt for mechanistic explanations for the reasons behind the measured differences. Actin is instrumented in wound healing as well as during tumor metastasis; it is also the most important protein in heart and other muscle function. Very few drugs currently modulate actin activity directly, albeit the abundant availability of anti-inflammatory medications which affect the COX pathway. In the literature on cell biology, through the input and examples provided by my colleagues (accompanied by their suggestions to apply my quantitative tools), I have identified discrepancies in the perception of actin behavior, especially in regard to the areas on the interface of the lamellipodium and the lamella (the lab of my dissertation adviser had reported similar interactions at the edge of contact-inhibited cells) in epithelial cells and at the base of the neck of growth cones during neuronal migration. The phenomena quantified and reported in this manuscript were first observed by the experimentalists who acquired the image series. It was their interest in having a way to measure, in great detail, the variability in cellular response to treatment that triggered this work. What has been of a particular interest to me, because of considerations of modulating contractility in disease, is the precise quantification of the regional variability in the dynamics of polymer networks in living cells, which are considerably more interdigitated than initially perceived and reported in the literature.

The new imaging data, generated specifically for this manuscript, was meant to allow my software to present its ability to measure multiple overlapped coherent flows, as the algorithm is not limited to just two flows. To obtain such datasets, I asked my colleague Andrea Bacconi if he could perform a perturbation that would disturb the actin meshwork to the point that many (three or four) crisscrossed networks would be formed. He replied: “Yes, tropomyosin”. Quantitative tracking in the images he acquired revealed that the over-expression of the long and short human isoforms of tropomyosin led to somewhat opposite effects on the speeds and level of heterogeneity in the anterograde and retrograde actin flows they generated. This result has implications for the treatment of diseases of the gut as well as the heart. Further investigation using tropomyosin inhibitors could identify the additional mechanisms of cytoskeletal regulation which cells activate when actin function is impaired. My hypothesis is that targeting actin in resistant tumors could sensitize cancer cells to tubulin inhibitors. If this proves true, it will have implications in the clinic.

1. ABSTRACT

The complex dynamics of cytoskeletal meshworks make them a difficult subject of study. With the advent of fluorescent speckle microscopy (FSM) and other technological advances in microscopy techniques, much more is now known about how the filamentous actin (F-actin) and MT networks work within cells to give rise to the vast array of functions which require them. A current challenge to the imaging field is to improve the utility and accuracy of the computational approaches required to analyze large and complex imaging datasets. Here, we present the results of a computational method that, when applied to FSM time-lapse series, can capture the instantaneous state of the rapidly changing, dense, and multi-directional speckle flows often exhibited by cytoskeletal dynamics in living systems. Re-analysis of previously published FSM image sets demonstrates that this method, which we call the Instantaneous Flow Tracking Algorithm (IFTA), can accurately detect speckle flows in mitotic spindles and F-actin meshworks, even in regions of high dynamicity of overlapping, anti-parallel flows where previous methods failed.

The anti-parallel flow at the metaphase plate of the mitotic spindle is a well-known phenomenon during the initial stages of chromosome segregation and it has been measured by several approaches, mostly in stationary spindles which do not exhibit any polar rotation. The mitotic spindle is the target of many cancer and neurodegenerative drugs and as such, there has been many attempts at inhibiting its basic functions with the objective of preventing chromosome segregation and the formation of new daughter cells. Such attempts have largely been focused on the inhibition of the action of MT plus-end directed motors, for instance the kinesin Eg5. Spindles with inhibited kinesins have been thought to exhibit no MT flux, however IFTA measured regional flux of up to 2.7μm/min, which reveals the activity of potent secondary flux mechanisms. These results suggest novel, additional, approaches toward arresting cells in mitosis during patient treatment.

The traditional tracking methods erroneously measure zero flux in areas where contractile F-actin flows meet, denoted as a “convergence zone” and commonly found in the lamella of motile cells and the neck

of growth cones. When IFTA was used to analyze FSM datasets derived from these structures, we detected high rates of protein turnover, anti-parallel speckle motion, and fast flux of actin subunits in both directions in the same “convergence zones”. This demonstrates the presence of a molecular machinery based on contractility in the lamella/lamellipodium of migrating cells and at the base of growing neurons, which can be exploited in the clinic. When applied to FSM data of migrating kangaroo rat kidney epithelial Ptk1 cells over-expressing different isoforms of the actin-based motor tropomyosin, IFTA revealed distinct, isoform-specific effects on contractile F-actin flows. Specifically, we found that decreased affinity between tropomyosin and F-actin correlated with an increase in speckle velocity heterogeneity. Such quantitative imaging analysis offers the ability to reliably test novel therapeutics *ex vivo.*

In summary, our results demonstrate that IFTA is a valuable tool that, in contrast to other existing trackers, can accurately resolve the complex, yet organized dynamics of interconnected polymers of cytoskeleton proteins, such as tubulin and actin.

2. INTRODUCTION

Quantitative analysis of FSM datasets provides a powerful means to probe molecular mechanism, but resolving speckle motion poses numerous challenges. Fluorescent speckles, sub-resolution cluster of fluorophores, are often faint and unstable, and typically present in only a few images of a time-lapse sequence (*1*). Their motions can be entangled and fast-evolving, especially in complex cytoskeleton structures where large numbers of speckles move in an organized fashion in multiple directions as a part of overlapping speckle flows. Recently, we proposed a new method, which we abbreviate as IFTA, based on graph theory which can be used to establish correspondence between speckles in time-lapse image sequences (*2*). Specifically, IFTA computes multiple vector flow fields based on knowledge of the regional organization and local smoothness of speckle motion (*2*) by considering three consecutive frames of an image sequence at a time. Thus, the method allows us to consider not only the displacement of speckles but also the local curvature and acceleration of their trajectories. This leads to a more accurate assignment of correspondence between speckles in consecutive frames. Additionally, we apply bi-objective optimization where the maximization of the number of accepted links between speckles competes with the global cost (computational penalty) of linking particles. During building the graph solution, when candidate matches form unusual triplets, because of the direction or speed of motion, these links are assigned a higher cost and thus become more likely to be excluded in the selection. Naturally, the two goals of forming as many links as possible at the lowest cost are contradictory, as maximizing the number of links requires an increase in overall cost while minimizing the overall cost requires a decrease in the number of links. This is a key novelty in our approach, which guarantees, mostly critically, the elimination of any false positive links. The generation of false positive tracks has been the most important flaw of all previous tracking approaches used in the scenarios we consider. It creates the issue of delivering wrong flow information and, this way, leads to conclusions regarding cell behavior which do not correspond to the actual processes in living cells. The contribution of IFTA consists of its unique ability to identify organized motion of cohorts of speckles, while removing of the

measurements speckles which do not belong to a specific group. That is to say that, for instance, if we measure a cell with four flows which move in different directions and there is a fifth group of speckles which undergo unstructured motion, IFTA will dissect the behavior of these four speckle flows, while leaving out the fifth group. The way our solver is built, IFTA only incorporates in its measurements speckles belonging to a cohort, assuming the speckles move in a similar way, i.e., in the same direction and with the same speed. The cut off values for accepting a speckle within a flow are assigned dynamically based on a Bayesian rule and the posterior distribution of each of the components of the cost function, which is updated at every step of an iterative procedure.

For visualization purposes, we have applied wide directional averaging of the displayed in the figures vectors in order to observe the overall differences in the angular orientation of the flow fields, which is the main novelty. This filtering comes at the expense of smoothing the local curvature, which is not so clearly observed in the images presented, however, this visualization parameter can be easily modified to show better both the local speed and directionality. Our objective has been to convincingly demonstrate that there are unappreciated cellular overlapped polymer flows which have not thus far been detected and measured. The histograms in all figures are, nevertheless, based on the unfiltered vectors obtained from the clustering analysis after splitting the vectors resulting from the bi-objective optimization and therefore represent the true speeds for each of the tracked vectors.

IFTA does not overlink speckles and that leads to no false positive selections, while, by avoiding too stringent selections, we minimize the false negative selections. Thus, finding the optimal balance between the two optimization goals yields a robust tracking of contractile structures with an overall minimal number of false positives and false negatives at the same time. In contrast, existing speckle tracking approaches are not well suited for the analysis of contractile structures (*3-5*). Contraction occurs when anti-parallel MT bundles or F-actin branches lengthen or shorten in interdigitated polymer meshworks which are linked by molecular motors. Hence, cellular structures of the key characteristics studied in this paper and described below generate image datasets exhibiting frequent change of flux

speed and directionality on a short time scale. In principle, there is no limit to how many flows of different directionality can be analyzed with our method. In addition, IFTA is self-adaptive and requires no *a priori* knowledge and user input regarding motion velocity.

In all examples shown here, earlier tracking approaches have been unsuccessful to resolve in fully automated fashion anti-parallel flux of interdigitating cytoskeletal networks when cohorts of speckles constitute coherent overlapping flows. These approaches also fail when confronted with speckle flows that exhibit twist or curl, a situation encountered when cytoskeletal networks flow around fixed objects within the cell or when the activity of molecular structures is inhibited. Therefore, we propose using IFTA as a quantitative tool for the analysis of sub-cellular areas with anti-parallel and overlapping filamentous polymer networks which is capable to precisely measure the instantaneous change of flow directionality and rapid increase or decrease of velocity of MT flux. We consider the strengths of IFTA of particular importance for the evaluation of novel cancer and neurodegenerative compounds. Such drugs modulate the cytoskeleton, sometimes in unexpected ways, and the ability to reverse impaired cellular functionality in disease pre-determines their efficacy in a clinical trial. Failure to rigorously probe novel compounds in functional assays has been the reason for poor drug-candidates secondary screening, which, in turn, leads to low cure rates in the clinic. Our observation is that this failure is not the result of bad experimental approaches but rather errors in thoroughly quantifying the available imaging data. These errors stem largely from a lack of specialized computer vision tools required to dissect the incredibly complicated scenarios encountered in the biology of the cell in disease and during treatment.

The main discoveries presented in the manuscript, based on published and newly generated imaging data, are related to the ability of the cell to adapt to a wide range of biochemical and mechanical perturbations. We have investigated this in the context of the two main cytoskeletal proteins, tubulin and actin. Tubulin has been the target of numerous therapeutic approaches for six decades now. Most of these therapies have been, in essence, a “black box” approach, where a treatment with debilitating side

effects is administered, without having the ability to anticipate whether it would affect the desired target. In this manuscript, a quantitative evaluation of some of the more difficult to interpret effects of tubulin-targeting compounds has been reported together with an attempt for mechanistic explanations for the reasons behind the measured differences. Actin is instrumented in wound healing as well as during tumor metastasis; it is also the most important protein in heart and other muscle function. Very few drugs currently modulate actin activity directly, albeit the abundant availability of anti-inflammatory medications which affect the COX pathway. It is the variability of patient response in genomics precision medicine that underscores the importance of utilizing quantitative imaging techniques in the clinic. A plethora of the cellular proteins exhibit ambiguity in function and response to perturbations. There exists a high level of regional variability in the dynamics of polymer networks in living cells, which are considerably more interdigitated than initially perceived and reported in the literature. Drugs bind to proteins within these networks and affect their function. Consequentially, the modulation of MT and F-actin dynamics and contractility inevitably affects drug efficacy. Answers about the potential efficacy of a drug can, thus, be obtained by developing software systems that measure, in great detail, the effects of a regimen on its cellular targets. Molecular manipulations of living patient-derived cells *ex vivo* can reveal which secondary mechanism would be activated after a particular intervention. Such clinical research can aid the discovery of an optimal drug selection for each disease, which is the motivation for this work.

3. RESULTS

3.1 Tracking Spindle MT Movements

MTs constitute the major structural element of the mitotic spindle. Within this bipolar, fusiform structure, inherently polar MTs are typically oriented with their minus ends, from which tubulin dimers dissociate, pointing toward the pole and their plus ends, where tubulin dimers are added to the MT lattice and begin moving toward one of the poles, pointing toward the midzone. This spatial organization creates a region of predominantly anti-parallel MT overlap within the central part of a bipolar spindle where MT-based motor proteins, such as heterotetrameric kinesin-5 (Eg5 in *Xenopus*), cross-link and slide MTs resulting in slow poleward transport of MTs (*6, 7*). Termed "flux", the abovementioned movements can be visualized by FSM (*8*). The anti-parallel flux in the central spindle represents a difficult, yet well-characterized tracking problem. There are important subtleties (*9*), however, in the organization of the spindle, such as the slower flux in kinetochore MTs compared to non-kinetochore MTs, which remain largely unexamined. Statistical analysis of large populations of speckles can deliver insights regarding the differences in the distributions in question when the underlying analysis extracts the correct data vectors. When the data is analyzed without the necessary motion models and optimization techniques, false positive links lead to the incorporation of unexisting motion components and that, in turn, leads to inability to distinguish faint differences between two flow distributions. Reporting such differences becomes very important in disease and during patient treatment as novel regimens affect differentially the variety of MT subpopulations depending on function and regulation.

It becomes even more challenging for the traditional techniques to measure flows in multipolar spindles in cancer cells. Spindles which progress to anaphase without forming a bipolar structure result in aneuploidy. IFTA was successfully tested to resolve the flows in a tripolar spindle in a *Xenopus egg* extract (data not shown), which was accidentally formed when several MT bundles had glued to the cover slip, thus forming artificially a third pole. Our algorithm can resolve any number of overlapped

flows, which can be valuable when testing the effects of novel therapies to, for instance, affect multipolar spindles selectively.

3. 1. 1. Anti-parallel MT flux in wild type mitotic spindles

As an initial test of IFTA, we used our algorithm to measure MT flux rates in "cycled" spindles assembled in *Xenopus egg* extracts (*10*), some of which form about three thousand speckles at each time point. IFTA-measured flux velocities were similar for FSM datasets acquired using either widefield or spinning disk confocal fluorescence microscopy (2.02 ± 0.73µm/min and 2.21 ± 0.81µm/min respectively) and comparable to published rates measured using linear Kalman filtering (*4, 11*) (2.52 ± 0.65µm/min), photoactivatable tubulin analogues (*12*) (2.90 ± 0.40µm/min), or correlation-tracking (*13*). Thus, even though IFTA represents a fundamentally different tracking strategy, these data demonstrate that the approach can both detect and accurately measure spindle MT flows. IFTA is readily able to detect opposing speckle flows in the spindle midzone (Fig. 1A).

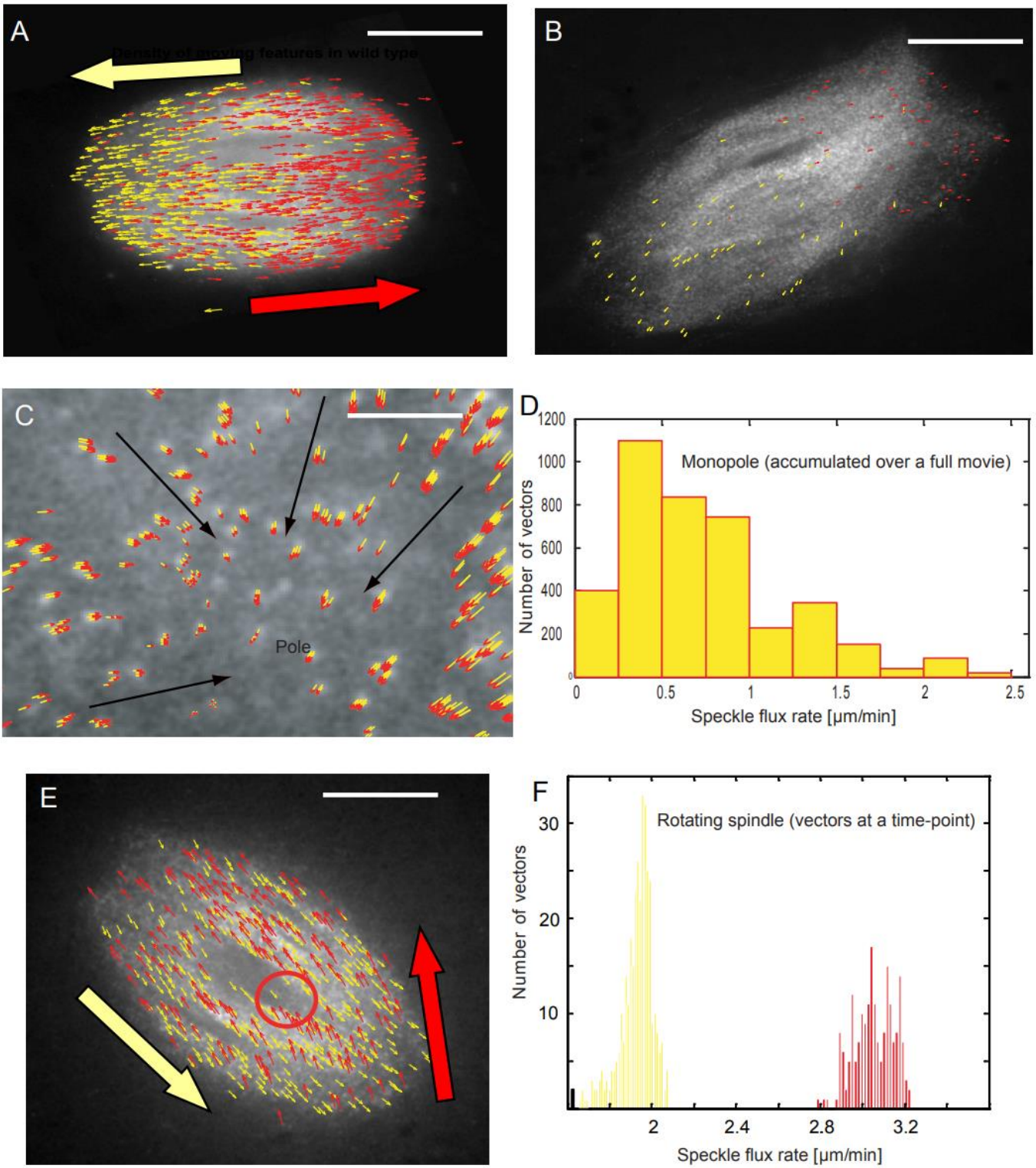

Figure 1. IFTA Analysis of Spindle MT Dynamics in *Xenopus Leavis* Egg Extracts. IFTA was used to track bi-directional MT polymer flux in metaphase spindles in *Xenopus egg* extracts as imaged using fluorescent speckle microscopy (FSM).

Figure 1A (scale bar equals 5µm) shows a single FSM image of labeled-tubulin speckles from an FSM time series (untreated spindle image datasets were taken from reference *19*) which has been overlaid with flow vectors generated using IFTA. Two opposing flows were detected and clustered based on their distinct directionalities toward each of the two spindle poles (shown in red and yellow vectors). Note the large spatial overlap, particularly in the spindle midzone, between the opposing flow fields. The main flux directions detected are marked with a red arrow, toward the right pole, and a yellow arrow, toward the left pole.

Figure 1B (scale bar equals 5µm). Bipolar spindles were imaged using FSM following the addition of 5mM AMP-PNP (a non-hydrolysable ATP-analog that inhibits MT-based motor activity), to spindle assembly reactions. This treatment has previously been reported to completely inhibit spindle MT flux while maintaining a bipolar spindle morphology (*14*) and we re-analyzed these image datasets. IFTA, in contrast, measured about 90% inhibition of MT flux. A small number of motion vectors (similarly to Figure 1A, shown in red and yellow to display vector direction of motion toward each of the two spindle poles), less than 130 out of over a thousand speckles in each image (about 10%), reported minimal MT movements. The average speed is 0.19µm/min, and the maximal speed is <0.61µm/min. Surprisingly, these localized speckle movements resembled slight contractions, resembling the way a snail crawls (see also Video 1, supplemental data), which seem to buckle some MT bundles. This suggests a residual motor activity in these spindles and potent contraction at several locations.

Figure 1C (scale bar equals 2µm) shows vector fields superimposed on FSM data of Eg5-inhibited monopoles (image datasets were taken from reference *17*). IFTA measured median flux rates of about 0.6µm/min in these structures (see also Video 2, supplemental data), with the fastest flux speeds being up to 2.7µm/min (see the histograms on Figure 1D). Vectors are drawn in black color to mark the inward speckle flow motion toward the pole of the monopolar spindle. The head of all individual speckle vectors are displayed in red to show the inward direction of the speckle motion. In the absence of active Eg5, this indicates the presence of MT sliding in extract monopoles with inhibited MT treadmilling. The results also indicate that other proteins are contributing to the generation of spindle MT flux, independent of Eg5 activity.

Taken together, the data suggests a secondary molecular mechanism, perhaps related to the activity of cytoplasmic dynein (*15*).

In Figure 1E (scale bar equals 5µm), IFTA was used to track speckle flow in spindles skewered with a single, vertical microneedle (image datasets were taken from reference *23*). Under these conditions, spindles slide parallel to their interpolar

axes and, at the same time, rotate continuously with velocities slightly slower than typically measured for flux, ultimately escaping the needle entirely. The red circle indicates the needle position and red arrows depict speckle motion away from the needle (toward the top of the image) whereas yellow arrows depict speckle motion toward the needle (i.e., toward the lower right corner of the image). These observations suggest that forces generated by flux are transmitted to the needle, hypothetically via MT cross-links that flow with the moving lattice. This means that MTs would flow around the needle at velocities equal to the velocity of flux within the spindle minus the escape velocity, i.e. $\bar{v}_1 = \bar{v}_{\text{flux}} - \bar{v}_{\text{spindle}}$, (yellow arrows pointing to the right and downward) while the velocity of flux in the opposite direction is increased to $\bar{v}_2 = \bar{v}_{\text{flux}} + \bar{v}_{\text{spindle}}$ (red arrows pointing up, in the direction of rotation).

The histogram of flow velocities (Figure 1F) shows two distinct velocity populations. The red population displays speckle motion away from the needle, with an average speed of over 3μm/min; in yellow is displayed the significantly slower (with 1.1μm/min or 37% slower), slightly over 1.9μm/min, speckle motion toward the needle. Because the flow fields rapidly change their directionality near the needle, a linear Kalman filter (*4*) links speckles across MT bundles and fails to accurately follow the local speckle motion by overestimating the speeds (data not shown). We studied nine such spindles and measured consistent significant difference in the average flow speed depending on flux direction, toward or against the direction of spindle motion (comprised of directional displacement and rotation of one of the poles, most commonly the pole further away from the needle) while escaping the needle.

These data demonstrate the extraordinary ability of the mitotic spindle to re-arrange and correct mechanical imperfections in its structure. The quantitative results indicate forces related to the extracellular matrix and molecular motors are driving these re-arrangements, rather than MT polymerization dynamics.

See Table 1 in Materials and Methods for further information regarding the conditions and perturbations.

3.1.2. Incomplete inhibition of MT flux in mitotic spindles after treatment with AMP-PNP

IFTA uses data-driven self-adaptive local and global speckle motion models (*2*). A well-known problem with computational tracking methods which apply motion models is the formation of false positive links between successive imaging frames when there is no actual motion. To benchmark IFTA and to test

whether it generates false positive links, we analyzed speckle flux in spindles treated with 5µM AMP-PNP (a slowly hydrolysable ATP analogue that inhibits MT-based motor proteins, mostly acting at the plus ends of MTs). This treatment inhibits spindle MT flux while maintaining a bipolar spindle morphology (*14*). In agreement with previous kymograph-based analysis (*6, 16*) and visual inspection (Video 1, supplemental data), IFTA detected only a small population of moving speckles suggesting little MT movement in these spindles and certainly no concerted flows (Fig. 1B, count <130, with average speed of 0.19µm/min and maximal speed <0.61µm/min). Interestingly, the roughly 10% of speckles which exhibited motion seem to show a contraction in several of the MT bundles (Video 1, supplemental data) oriented toward the corresponding pole of the spindle (Fig. 1B, the yellow vectors are in one half of the spindle and point toward the closer pole and the red vectors are in the other half of the spindle and point toward the opposite pole). This completely novel insight in the effects of AMP-PNP suggests a lower inhibition of cytoplasmic dynein at the minus ends of bundled MTs, even in areas of the spindle away from the poles. Such secondary mechanism may explain the limits of the potential use of AMP-PNP, and similar agents, like the Eg5 inhibitor ispinesib, in therapeutic applications. It points toward the need to combine compounds, such as the addition of a dynein inhibitor, and test their effects on patient-derived cells in the lab before any utilization in a clinical setting.

3.1.3. Residual MT flux in Eg5-inhibited monopoles

Small molecule motor inhibitors, like monastrol and S-trityl-L-cysteine, specifically target the flux-generating machinery by affecting the function of Eg5. Spindle assembly reactions in Eg5-inhibited extracts produce monopolar MT arrays whereas addition of these inhibitors to extracts with pre-assembled bipolar spindles results in spindle collapse into monopolar structures (*16*). Previous analysis of MT flux in Eg5-inhibited monopoles have yielded inconsistent results for measured average speckle speed. Image cross-correlation suggested insignificant flux rates of 0.2-0.3µm/min in Eg5-inhibited monopoles (*17*), leading to the conclusion that Eg5 motors are the sole drivers of flux in extract

spindles. Remarkably, when IFTA was used to measure flux rates in the same monopolar structures, the results indicate a median rate of about 0.6µm/min (Fig. 1C, Fig. 1D, and Video 2, supplemental data), with the fastest flux speeds being up to 2.7µm/min. Because IFTA did not detect flux for 90% of the speckles in AMP-PNP treated spindles, its detection of flux in Eg5-inhibited monopoles is likely not an artifact of the tracking algorithm and instead might indicate the presence of additional, Eg5-independent flux mechanisms. This is consistent with observations in mammalian tissue-culture cells where it was hypothesized that a reeling-in force, generated by spindle pole-associated MT depolymerases, also contributes to flux (*18-20*). Furthermore, the detection of flux in monopoles lends credence to spindle assembly models that inherently rely on MT transport to generate spacing between chromosomes and poles (*21*). Interestingly, flux in Eg5-inhibited monopoles measured using IFTA is similar to that detected in the "polar MT bundles" that remain following treatment with Op18, a MT-destabilizing protein that selectively target the "barrel MT bundles" constituting the bulk of MT mass near the spindle middle zone (*11, 22*). It suggests, in both abovementioned scenarios, consistent cytoplasmic dynein activity.

3.1.4. Fast-evolving MT flux in mitotic spindle manipulated by microneedles (skewered spindles) exhibiting unpredictably twisting motion with rapid changes in directionality

A particularly well-suited application to demonstrate the unique capabilities of IFTA is the study of structural occlusions in the spindle which locally influence the usual poleward directionality of flux. Artificial inclusions can be introduced by skewering extract spindles with microneedles (*23, 24*). In previously published work, IFTA was used to make inferences regarding the mechanical properties of the putative spindle matrix (*23*). Spindles skewered in this way pushed themselves off the needle by moving parallel to their interpolar axes at velocities slightly slower than typical flux rates, ultimately escaping the needle entirely (*23*). These observations suggested that forces generated by flux are transmitted to the needle, hypothetically via MT cross-links that flow with the moving lattice. This

means that MTs would flow around the needle (red circle on Fig. 1E) at velocities equal to the velocity of flux within the spindle minus the escape velocity, i.e. $\bar{v}_1 = \bar{v}_{\text{flux}} - \bar{v}_{\text{spindle}}$, (Fig. 1E, yellow arrows) while the velocity of flux in the opposite direction is increased to $\bar{v}_2 = \bar{v}_{\text{flux}} + \bar{v}_{\text{spindle}}$ (Fig. 1E, red arrows; see also the clearly separated speed distributions in Fig. 1F). Similar to a flag in the wind, in these experiments, external flows in the *Xenopus egg* extract often caused spindles to rotate around the skewering needle. In addition, because the flow vectors rapidly change their directionality near the needle, linear Kalman filtering (*4*) links features across fibers and fails to accurately follow the local speckle motion (data not shown). We studied nine such spindles and measured consistently significant differences in the average flow speed depending on flux direction (Fig. 1F), toward or against the direction of spindle motion while escaping the needle. In all spindles the concrete trajectory of overall motion was very different and for all spindles IFTA could accurately follow every step of the ever-changing spindle location. Therefore, IFTA is the algorithm of choice to measure instantaneous fast-evolving overlapped flow fields of cohorts of speckles participating in multi-directional organized motion. Our method has also particular strength and robustness when the data pose substantial challenges in terms of spatiotemporal variation of speckle behavior within the flow field, as well as speckle appearances and disappearances. IFTA captures the instantaneous organization of the speckle flows by balancing the number of speckles linked with how well those links conform to the overall motion of the speckle flow they are assigned to. The trade-off between the numbers of links formed versus the overall cost (where a lower cost is a measure of similarity) of linking is accomplished by performing bi-objective optimization between the local and regional motion models; it can be imposed adaptively to the continuously changing speckle dynamics. Thus, any re-organization in the overlapping speckle flows is captured and measured by using as few as three consecutive images. Therefore, IFTA will be very suitable for analysis of MT flux at another very delicate stages of cell division, prometaphase and the onset of anaphase. At these stages, the spindle behavior is somewhat similar to that of the skewered spindles described in this section. Namely, the flux

in a portion of the MT bundles suddenly accelerates leading to irregular patterns of speckle flow fields and, in some cases, rotational motions and rocking of the spindle. The spindles rapidly change position for a short period of time, in a similarly unpredictable manner, before continuing into the following stage of cell division.

These data demonstrate the extraordinary ability of the mitotic spindle to re-arrange and correct mechanical imperfections in its structure. The quantitative results indicate forces related to the extracellular matrix and molecular motors are driving these re-arrangements, rather than MT polymerization dynamics. The implication of these measurements is that even the maximum tolerated dose of docetaxel, which does not arrest in mitosis all spindles but rather many, would allow for a few tumor cells to proliferate. As an example, in prostate cancer, most tumors are heterogeneous and dormant – until they are treated. After initially receding, the tumors resume growing. Further, this process would effectively serve as a repeated selection step, allowing for the replication of the most resilient clones. Taken together, the data indicates the level of difficulty in interfering with mitosis by modulating cytoskeletal polymers without inhibiting the action of specific plus-end and minus-end directed motors as well as proteins providing mechanotransduction in the tumor microenvironment.

3.2. Tracking Contractile Actin Flows in Fluorescent Speckle Microscopy Data

Similarly to spindle MT arrays, F-actin filaments are often arranged in anti-parallel contractile fibers or in more complicated contractile meshworks, for example near the leading edge of migrating cells. Cell migration is powered by a coordinated cycle of leading-edge protrusion in the direction of migration, substrate adhesion of the protrusion, generation of tension on new focal adhesions (FAs) to advance the cell body, and de-adhesion of the trailing cell rear. F-actin is required for each step of the cycle. Spatio-temporally coordinated regulation of the interaction of F-actin with specific binding proteins and myosin motors is required for the actin cytoskeleton to perform such diverse mechanical functions. Because of a

lack of appropriate image analysis methods, the dynamics of contractile F-actin structures has been understudied. We, therefore, proceeded and tested the applicability of our IFTA to the investigation of contractile arrangements followed by rapid F-actin meshwork re-arrangements in migrating epithelial cells and similarly highly dynamic neuronal growth cones.

3.2.1. Anti-parallel actin flows in the "convergence zone" between lamella and cell body in migrating epithelial cells

Anti-parallel F-actin flow is immediately expected in migrating cells. Retrograde flow of the dendritic F-actin network in the lamellipodia meets the anterograde flow of cell body F-actin in the so-called "convergence zone", resulting in anti-parallel F-actin movements and/or F-actin depolymerization. To test whether overlapping contractile F-actin flow patterns exist in normal migrating cells, we re-analyzed previously published FSM datasets of PtK1 cells. Previous analysis of F-actin dynamics (*3*) identified the presence of two anti-parallel F-actin flow fields: retrograde flow in the lamella and lamellipodia, and forward F-actin movement in the cell body (*25*). Disappearance of flow vectors in the so-called "convergence zone", where the two anti-parallel flow fields meet, was interpreted as F-actin disassembly, and previous tracking methods have not provided evidence of any anti-parallel (contractile) F-actin movement in the "convergence zone". However, visual inspection of these FSM image sequences shows that the method fails to correctly track direction and speed of overlapping F-actin flows (yellow vectors on the inset at the upper right corner of Fig. 2A). In contrast, our IFTA tracker found a considerable overlap of the two interdigitating networks and specifically emerging anti-parallel flows in intracellular regions previously thought to be zones of F-actin depolymerization (side-by-side comparison is presented in Fig. 2A and the inset with yellow vectors at the upper right corner of the figure). In the area marked with a red circle, similarly to (*25*), we measured a dense anterograde flow of about 2μm/min. In the area thought to be convergent with no flux, we measured two overlapped networks, an anterograde flow (in red vectors) and a retrograde flow (in yellow vectors). It is of

significant difficulty to detect any zone of absolute flow convergence in this dataset, i.e., an area of no speckle flux and diffusion of free dimers, as suggested by the measurement depicted by the short speed vectors (in yellow color on the inset) of length close to zero in Fig. 2A (inset taken from reference *25*). Thus, although F-actin depolymerization certainly occurs in the so-called "convergence zone" and previously measured depolymerization rates are likely largely overestimated. The reason for this error is that anti-parallel flow fields cancel each other out when regional vector filtering is performed, during the iterative data processing, in previous tracking methods (*25*). Remarkably, our measurements showed that the two, a retrograde and an anterograde, interlaced speckle flow fields are extending way beyond the so-called "convergence zone". Our method shows that the two anti-parallel actin speckle flows are clearly interdigitating and fluxing in opposite directions in the areas of overlap, thus suggesting these areas are significantly contractile.

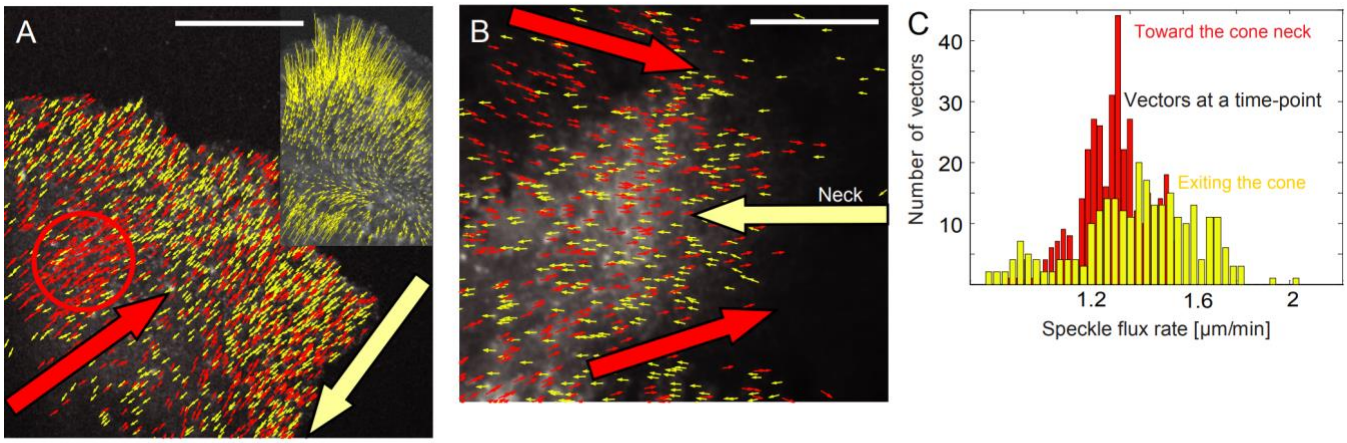

Figure 2. Actin Networks with Anti-Parallel Speckle Flows. IFTA was used to track bi-directional F-actin polymer flux in migrating kangaroo rat kidney epithelial PtK1 cells and growth cones in primary cultures of Aplysia bag cell neurons as imaged using fluorescent speckle microscopy (FSM).

Figure 2A (scale bar equals 5μm). **Contractile actin networks**. We measured a considerable overlap of the two interdigating networks and, specifically, emerging anti-parallel flows in intracellular regions previously thought to be zones of F-actin depolymerization (side-by-side comparison is presented in the inset of this figure). It is of significant difficulty to detect any

zone of absolute convergence in this dataset, i.e. an area of no speckle flux and diffusion of free dimers, as suggested by the measurement depicted by the speed vectors of length close to zero inset (with yellow vectors showing no flux in the so-called "convergence zone", based on an earlier analysis over the full movie) taken from reference *25*. The tracking method used in (*25*) cannot handle anti-parallel motion and vectors with opposite directions, belonging to opposing flow fields. cancel out when directional filtering is performed during data postprocessing. This inaccuracy in quantification has so far been interpreted as local depolymerization activity. Using IFTA, we can now reliably measure that depolymerization rates in the "convergence zone" are significantly lower than previously appreciated.

Figure 2B (scale bar equals 10µm). **Anti-parallel flux in the base of growth cone**. The flows in the two directions have different speeds, the retrograde flux is on average slower but more homogenous (see Figure 2C). The image datasets were taken from (*26*). In growth cones two anti-parallel F-actin networks are thought to merge at the base but visual inspection points at slight contraction (see also Video 3, supplemental data). Growth cones have a "convergence zone" near the axonal shaft and previous analysis have not resolved the actins flows at the so-called neck of the cone. We found that the anterograde and retrograde flows interdigitated and flux with different speeds in the range of 1 to 3µm/min. The anterograde flow passing through the neck of the growth cone was oriented straight toward the center of the leading edge exhibiting high level of speed heterogeneity (yellow arrows on Figure 2B and yellow bins on Figure 2C). Oppositely, the retrograde flow showed narrow (and also slower on average) speed distribution but a heterogeneity in terms of angular orientation, as the F-actin translocation followed the outer shape of the cell (red arrows on Figure 2B and red bins on Figure 2C).

See Table 1 in Materials and Methods for further information regarding the conditions and perturbations.

3.2.2. Anti-parallel actin flows in the "convergence zone" at the base of neuronal growth cones

In neuronal growth cones, the F-actin network is organized similarly to the front of migrating cells and we next asked whether IFTA can dissect the arrangement of contractile F-actin networks in migrating neurons. In growth cones, two anti-parallel F-actin networks are thought to merge at the base (*26*) but visual inspection of published data shows contraction at the narrow entry point at the neck of the growth cone (Video 3, supplemental data). Thus, a "convergence zone" was thought to exist near the axonal shaft as previous analyzes ((*27*), see Fig. 2B) have not been able to measure the velocities of the F-actin

flows at the growth cone neck. Using IFTA, we were able to identify clearly present anterograde and retrograde flows which were interdigitated. We measured heterogeneous flux rates with a plethora of actin speckle speeds, in the range of 1 to 3 μm/min (Fig. 2C). The anterograde flow passing through the neck of the growth cone was oriented straight toward the center of the leading edge exhibiting high level of speed heterogeneity (Fig. 2B, yellow arrows pointing to the left with a distribution shown in yellow on Fig. 2C).

Both results have a very intuitive interpretation as, at the cone, the F-actin polymer meshwork translocates from a narrow zone of high density of parallel speckle motion to a wider zone within the growth cone, hence the vectors are mostly parallel, yet speckles move at high variety of different speeds. Oppositely, the retrograde flow showed narrower slower on average speed distribution (i.e., the high-speed speckles were suppressed) but with a high level of heterogeneity in terms of angular orientation, as the F-actin translocation followed the outer shape of the cell (Fig 2B, red arrows pointing to the right with a distribution shown in red on Fig. 2C). These results are also intuitive in terms of geometrical interpretation as polymerization rates (i.e., speckle motion speeds) equalize at the entrance of the neck of the cone and, at the same point of entry, the wider network becomes narrower, hence the higher angular homogeneity of the F-actin network entering the neck.

Besides F-actin networks in growth cones in control cells, we analyzed cells after addition of 70 μM blebbistatin. Blebbistatin is a small molecule inhibitor which inhibits the activity of myosin II. After treatment, we measured slower F-actin turnover rates and a reduction of the anti-parallel contractile motion in perturbed cells (data not shown). Again, this result seemed very intuitive given the effects myosin II filaments exert on the actin organization. This provided us with confidence that IFTA can truthfully detect shifts in velocity, both for changes in the speeds and spatial orientation, for a complex organization of flows.

3.2.4. Contractile multi-directional actin flows in the "convergence zone" in the area between the lamella and lamellipodia of epithelial cells with over-expressed tropomyosin-2

Tropomyosins are long coiled-coil dimers that bind along F-actin filaments. In muscle cells, tropomyosins modulate myosin binding and activity (*28, 29*). In non-muscle cells, increased amounts of tropomyosin alter lamella and lamellipodia dynamics (*30*), but the underlying molecular mechanisms and, to what extent different tropomyosin isoforms differently affect F-actin dynamics, are not understood. Anti-parallel F-actin flow is myosin-mediated, and it is reasonable to assume that tropomyosins could regulate myosin-mediated anti-parallel F-actin contractions. Indeed, excess tropomyosin in migrating cells has previously been shown to render the F-actin network hyper-contractile (*30*). We, therefore, used our novel tracking method to test how different tropomyosin isoforms modulate F-actin dynamics. Concretely, we over-expressed two tropomyosin isoforms, one from the α-gene (tropomyosin-2 (Tm2)) and one from the δ-gene (tropomyosin-4 (Tm4)) in PtK1 cells. Visually, we observe highly dynamic, re-organizing F-actin networks. We first applied a tracking method used in (*30*) for actin speckle flow measurements to successfully detect and decouple the effects of oppositely organized F-actin meshworks (*31*). It failed to measure the speeds in the area of overlap and displayed speed vectors of, close to, zero (data not shown) as described in section 3.2.2. above. Also, in both cases of over-expression of the two tropomyosin isoforms texture-based tracking (*5*) yields no interpenetrating speckle fluxes (see the insets with yellow vectors in Fig. 3A and Fig. 3C). We then used IFTA to quantify the effects of tropomyosin over-expression on F-actin dynamics. First, using IFTA, we measured that Tm2 overexpression increases the speed of F-actin flux by about 30%, with speeds ranging from 1.9um/min to 2.5um/min, while preserving the organization of F-actin in retrograde and anterograde flows interdigitating at the so-called "convergence zone". Exceptionally, we identified examples of four overlapping flows in cells overexpressing Tm2 (Fig. 3B, see the speeds of four vectors flows in the color histogram) which seemed to be coupled in orthogonal pairs (Video 4, supplemental data). None of the four speckle flow fields was a result of stage drift. We established that there are four

significant flows by using expectation-maximization based automated selection of the number of vector cluster directions (*2, 32*). Two of the flows exhibit perpendicular to each other anterograde type of motion (in magenta and yellow in Fig. 3A and Fig. 3B) with faster flow speeds and higher level of heterogeneity and standard deviation of the speed distributions. Oppositely, the two retrograde flows (in red and green in Fig. 3A and Fig. 3B) have slower and narrower speed distributions. Those two flows (the one represented with red arrows on Fig. 3A in particular) seem to stem from overall underlying polymer translocation rather than active F-actin meshwork activity. Their speed distributions have lower standard deviation, the reason for which might be that the whole structure is moving, and with that translocation, all speckles move with very similar speeds. This observation, together with the high edge activity, compared with wild type (control) cells, suggests that Tm2 plays an essential role in the rapid remodeling of F-actin filaments at the edge, yet preserving the shape of the speed distributions. Tm2 acts as an F-actin filament stabilizer and the long F-actin filaments decorated with Tm2 are stable and, therefore, can lead to the formation of protrusions in multiple directions.

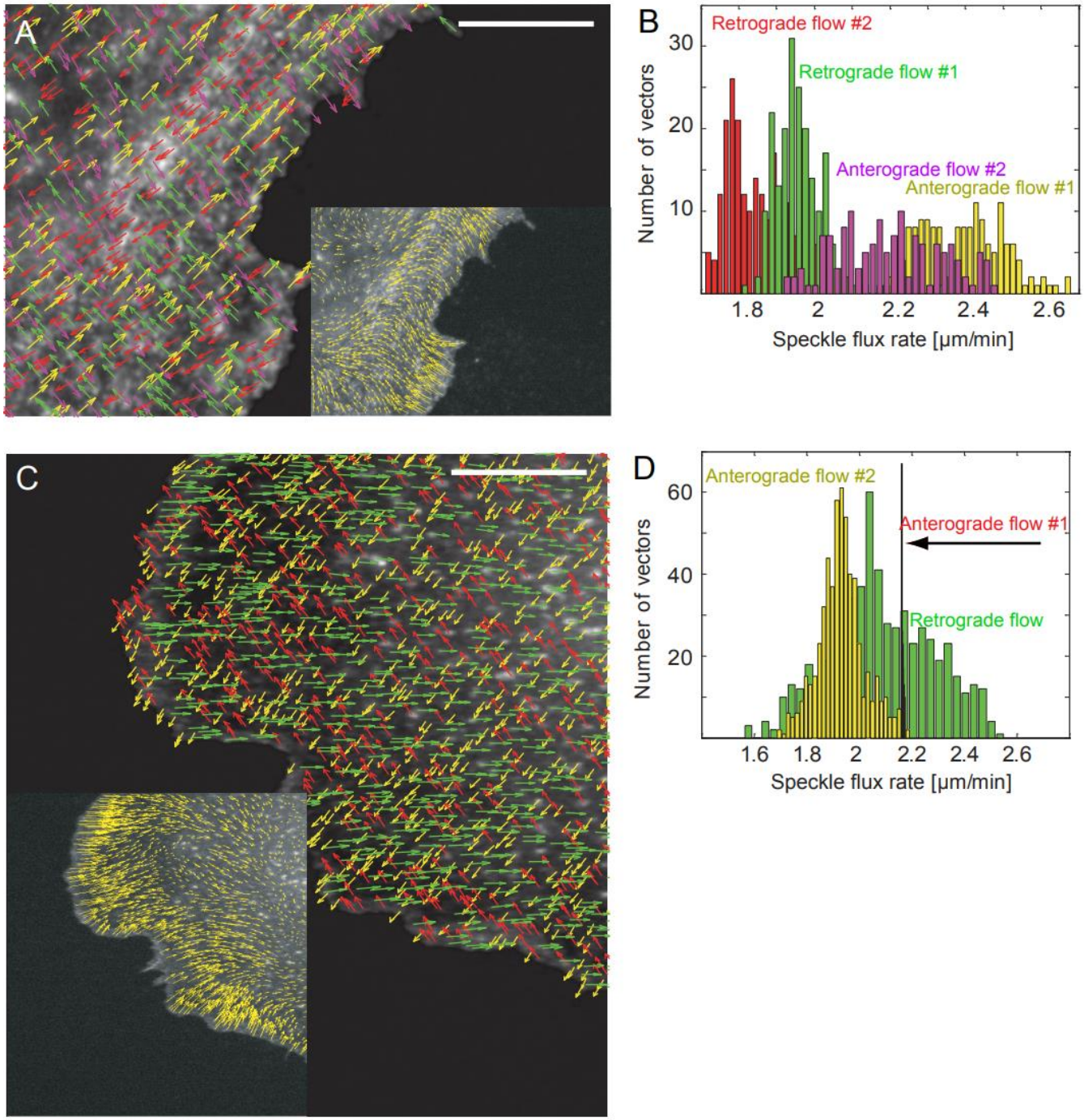

Figure 3. Highly Contractile Actin Networks: Over-expression of Tm2 and Tm4. IFTA was used to track four-directional and three-directional F-actin polymer flux in migrating kangaroo rat kidney epithelial PtK1 cells with over-expressed long (Tm2) and short (Tm4) human tropomyosin isoforms as imaged using fluorescent speckle microscopy (FSM).

Figure 3A (scale bar equals 5μm). **Tm2 over-expression increases anti-parallel left-right actin flux and leads also to anti-parallel up-down translocation, i.e., a four-directional actin flow.** We identified examples of four overlapping flows in cells over-expressing Tm2 (Figure 3B shows the corresponding four-color histogram) which seem to be coupled in pairs (see also Video 4, supplemental data). Two of these flow fields exhibit perpendicular to each other anterograde type of motion (in magenta and yellow vectors) with faster flow speeds and higher level of heterogeneity and standard deviation of the speed distribution (Figure 3B). Oppositely, the two retrograde flows (in red and green vectors) have slower and narrower distributions; those two flows (the one represented with red arrows in particular) seem to stem from an overall underlying polymer translocation rather than an active F-actin meshwork activity as the speed distributions have lower standard deviation, the reason for which might be that the whole structure is moving and, thus, all associated speckles move with very similar speeds. This observation, together with the high edge activity, compared with wild type cells, suggests that Tm2 plays a role in the fast remodeling of F-actin filaments at the edge, yet preserving the shape of the speed distributions. Tm2, thus, works in this scenario like an F-actin filament stabilizer and long F-actin filaments decorated with Tm2 are stable and, therefore, can lead to the formation of protrusions in a different direction. In comparison to IFTA, texture-based tracking (*5*) yielded no interpenetrating speckle fluxes, but rather displayed vectors of a retrograde flow at the cell edge and a zone of no flux in the lamella, both of which are incorrect (see the inset with yellow vectors on Figure 3A).

Figure 3C (scale bar equals 5μm). **Tm4 over-expression makes actin flux more heterogeneous**. In the case of Tm4 over-expression, actin speckles often exhibit two peaks in the distribution. The two "waves" of speckles resemble a distribution in which, first, there is a distribution similar to the wild type speeds and then, there is a second faster peak centered around the average F-actin flux speed for data with over-expressed Tm2. Hence, many of the Tm4 over-expression datasets demonstrated an incorporation of both a wild type behavior and a Tm2 over-expression behavior. We also observed that while the retrograde or anterograde speeds of the F-actin flows were increased with the over-expression of Tm2, the over-expression of Tm4 created visibly different flow patterns with multi-directional flows where a sub-population behaves like wild type, while another one moves faster and in a distinctly heterogeneous way. Tm4 is a weaker actin binder and therefore its over-expression can stabilize nascent F-actin filaments. In the histogram shown on Figure 3D (in three colors – green, red, and yellow), one can observe the very narrow peak formed by a flow moving parallel to the cell edge (red arrows and red bins). Remarkably, with values ranging 2.17-2.18μm/min, there is a clear indication of a highly organized motion with extremely narrow speed and angular variation and standard variation. In comparison to IFTA, texture-based tracking (*5*) yields no interpenetrating speckle fluxes, but rather displayed vectors of a retrograde flow at the cell edge and a zone of no flux in the lamella, both of which are incorrect (see the inset with yellow vectors on Figure 3B).

Overall, in contrast to Tm2 over-expression, the retrograde flow (in green color on Fig. 3C and Fig. 3D) is faster than the anterograde, ranging from values lower than the anterograde to significantly faster. The over-expression of the Tm4 isoform, the more transient actin binder, however, has lesser effects on the organization of the retrograde F-actin meshwork, i.e., a smaller number of organized retrograde flows are present, yet all of them exhibit an increased heterogeneity of the distribution of speckle flux speeds suggesting that Tm2 over-expression fragments at a higher degree the F-actin flows (for instance, resulting in four overall actin flows, from the wild type two flows). Another difference between the two isoforms is that after an over-expression of Tm2, the anterograde flows are faster than the retrograde, while, oppositely, the over-expression of Tm4 leads to a slower anterograde speckle motion.

See Table 1 in Materials and Methods for further information regarding the conditions and perturbations.

3.2.5. Contractile multi-directional actin flows in the "convergence zone" in the area between the lamella and lamellipodia of epithelial cells with over-expressed tropomyosin-4

We also studied the effects of over-expressing Tm4, another isoform. In contrast to Tm2 over-expression, the retrograde flow is on overall faster than the anterograde, ranging from values lower than the anterograde to significantly faster in cells over-expressing Tm4. The retrograde or anterograde speeds of actin speckles for Tm2 over-expression data are normally distributed in a unimodal normal distribution which is faster than wild type data. Oppositely, in the case of Tm4 over-expression, actin speckles often exhibit two peaks in a bi-modal distribution. The two "waves" of speckle vectors resemble a distribution in which there is a first, slower, mode with a distribution similar to the wild type speeds and then there is an additional second, faster, peak centered around the average F-actin flux speed for data with over-expressed Tm2. Hence, many of the Tm4 over-expression datasets demonstrated actin dynamics of embedded both wild type behavior and Tm2 over-expression behavior. We also observed that even when the retrograde or anterograde speeds of the F-actin flows were increased (like in the case of over-expression of Tm2), Tm4 often created distinctly different flow patterns of three-directional flows, some of which have sub-populations behaving like in wild type cells. In cells over-expressing Tm4, we often observed drastic directional changes in the flow organization

within the, up to, 10 minutes duration of the acquired movies; in contact, such changes never occurred in cells over-expressing Tm2. Tm4 is the weaker actin binder (*33*) and therefore its over-expression can stabilize nascent F-actin filaments, which might explain these interesting differences.

Remarkably, in the histogram shown in Fig. 3D (three color histogram distribution), one can observe the very narrow peak formed by a flow moving parallel to the cell edge (red arrows on Fig. 3B); with values ranging 2.17-2.18μm/min, a clear indication of highly organized motion with extremely narrow speed and angular variation. We did not observe any stage drift neither any movement of the cell body, therefore this measurement was not a result of an artifact, but rather represents a very interesting result demonstrating the ability of Tm4 to induce a very coordinated contraction parallel to the cell edge. This is measurement, which could serve as a quantitative readout in functional drug testing in the context of bone remodeling. Osteoclast activity is reduced with lowering the levels of Tm4, leading to the inhibition of bone resorption. Putative anti-aging compounds could be tested *ex vivo* for their ability to maintain a heterogeneous actin flows perpendicular to the cell edge, while inducing coordinated, fast polymer translocation in parallel to the cell edge. This quantitative assay could be used to evaluate compounds to treat and prevent diseases of the brain ranging from stroke to dementia.

In conclusion, the analysis of Tm2/4 data demonstrates that IFTA can detect differential effects of tropomyosin isoforms on contractility. Firstly, we concluded that over-expression of the Tm2 isoform, which is a stronger binder, causes a massive re-organization of the F-actin flows, resulting in flows in multiple directions with varying, narrower (for the retrograde flows) and wider (for the anterograde flows), speed distributions. Drugs to improve heart muscle and other muscle activity can be tested *ex vivo* based on this quantitative assay. Secondly, the over-expression of the Tm4 isoform, the weaker actin binder, which is a more transient binder, has lesser effects on the organization, i.e., causes a smaller number of organized flows, yet they seemingly exhibit an increased heterogeneity of the

distributions of speckle flux speeds. Drugs to improve bone repair and brain function can be tested *ex vivo* based on this quantitative assay.

The ability of IFTA to detect subtle differential effects in the organization of F-actin meshworks in areas of overlap demonstrates the power of this quantitative method. Overall, our analysis shows that, besides the two distinct F-actin networks driving the protrusion at the leading edge (*31*), in migrating cells there are also multiple, distinct contractile F-actin networks in the so-called "convergence zone" at the interface between the lamella and lamellipodia. Our work demonstrates the complexity of the mechanisms regulating the area of the cell where the cell edge ends and the cell body begins, and strongly suggests the existence of putative drug targets.

4. DISCUSSION

We have demonstrated the utility of IFTA for the resolution of multiple intersecting and/or interdigitating flow fields of fluorescent fiduciary markers, termed speckles. The goal of this contribution is to show examples of analysis of cytoskeletal dynamics where our approach resolves polymer fluxes that were missed by the global nearest neighbor (*3*), texture-based flow tracking (*5*), and projection-based particle tracking methods (*4*). The nearest neighbor method cannot handle high speed contractility measurements in high density networks. Such approach will always prefer to link speckles across the oppositely oriented polymers, thus erroneously resulting in short (close to zero speed) motion vectors and underestimated speckle speeds, and underestimated polymerization activity. The latter approach fails because of the latency of the linear Kalman filter required to propagate the motion of speckles between consecutive frames. Rapid flux changes either in space (change in direction) or time change in speed) are often missed. We have, therefore, previously used the IFTA to constrain the Kalman filter with information of spatio-temporal gradients in the instantaneous flow behaviors, which increased the tracking success rate from 61% to 96% (*4*). Finally, texture-based methods cannot cope with the task of tracking anti-parallel flows because of the averaging over multiple speckles in a region.

In summary, IFTA adds a new level of insight, in addition to the already available information about speckle flows measured by earlier tracking methods (*3*-*5*). Undoubtedly, those three methods performed accurately and robustly the speckle tracking tasks they were designed for. IFTA, however, brings in an additional strength as an add-on to those algorithms because of its capability to dissect specifically the cellular areas of active contraction, a key feature for many important cellular activities in disease. A technical shortcoming of IFTA, however, is that the algorithm extracts instantaneous flow behaviors but does not assemble full speckle trajectories. Hence, the method is not suited for measurements when speckle lifetimes, from “birth” to “death”, are required. Importantly, in the scenarios we presented, because of the rapid dynamics of the cellular polymers, the speckling fiduciary markers are only present

for three to four movie frames (10 to 20 seconds). For this reason, IFTA is well adept to extract all of the available information in these image datasets.

Until now, the accurate computational analysis of contractile cytoskeletal structures was limited due to the lack of appropriate software tools. Often speckle tracking in FSM images has been limited to the correct extraction of flow information at the cell edge up to the region of overlap of anti-parallel speckle flows. Since the entangled networks in the cell body are fast evolving, rapidly changing their turnover rates and directions of motion, it has been impossible for traditional tracking methods to resolve the anti-parallel motion. IFTA applies self-adaptive local and global motion models and is hence technically well equipped to analyze complex flow fields. Our method is very robust against frequent appearance and disappearance of speckles, as well as temporary occlusions, both characteristic of the dynamics in large contractile polymer structures with a significant turnover. This type of cellular flux measurements can add a new level of insight into contractile processes and advance our understanding of the dynamic organization of the cytoskeleton, cell division and motility, thus, advancing the field of drug development.

The over-expression of Tm2 and Tm4 demonstrates, in the new image data acquired for this manuscript, antagonistic effects on cellular contractility. The striking differences in the regulation of anterograde and retrograde F-actin meshworks, depending on the over-expression of the long or short isoform of tropomyosin, indicate potential applications of tropomyosin modulating medications in the regulation of heart function. Based on our analysis, Tm2 over-expression leads to retrograde flows with a narrow variation and anterograde flows with a wide variation in speed distributions. Oppositely, Tm4 over-expression leads to retrograde flows with a wide variation in speed distributions. Completely opposite effects we also measured in regard to the speed of F-actin flux in retrograde (faster when Tm4 is over-expressed) and anterograde (faster when Tm2 is over-expressed) flows. Therefore, it is conceivable that these antagonistic effects may allow for a precise tuning of muscle contraction beyond cardiac health but

also to improve athletic performance and recovery. Personalized drug options could be evaluated based on patient-derived cultures obtained from urine or skin samples with ease.

The role of tropomyosin regulation in kidney function underscores the importance of the *ex vivo* testing of novel compounds that affect the response to immunotherapy, such as drugs modulating the activity of the Glycogen synthase kinase 3 (*34*). Agents targeting this enzyme have been implicated in the treatment of a very wide variety of health conditions. Our results have implications for the treatment of diseases of the gut as well as the heart. Further investigation using tropomyosin inhibitors could identify the specific mechanisms of cytoskeletal regulation which cells activate in each case actin function is impaired or altered. Our hypothesis is that targeting actin in resistant tumors could sensitize cancer cells to tubulin inhibitors, which, if proven correct, will have implications in the clinic practice.

The potential clinical application of the analytics approach outlined in this manuscript pertains to anticipating drug resistance in cancer therapy and the treatment of neurodegeneration. Cell therapy is becoming the forefront of precision medicine, and it would be critical to be able to anticipate the mechanisms of action of the engineered immune cells. Natural killer cells and cytotoxic T cells employ different mechanisms to kill their targets, for instance by secreting cytotoxic lysosomes using the MT cytoskeleton for trafficking and release. There is also a plethora of effects induced in the target cells, most well studied of which lead to apoptosis and ferroptosis, a recently identified potent, caspase-independent, mechanism of programmed cell death. The exact pathways activated during therapy can be pinpointed by measuring its effects on the target proteins in patient-derived living cells *ex vivo*.

It is conceivable that for different patients, with overall very similar genetic profiles, a distinct type of engineered immune cells would be required. Given the availability of high-quality fundamental research equipment for high resolution live-cell microscopy in most university hospitals, what we propose is to embed in these systems real-time software for automated quantification and on-the-fly statistical analysis of intracellular behavior. Introducing this quantitative imaging method to the clinic would allow physicians to fine-tune, with a high level of certainty, an optimal treatment regimen for each patient.

5. MATERIALS AND METHODS

5.1. Sources of FSM datasets

Most of the image datasets presented in this paper were generated previously and computationally analyzed with earlier tracking methods in the context of several publications (Table 1). The new imaging datasets prepared specifically for this work is the tropomyosin perturbation data, as these datasets exemplified in a compelling way the specific strength of our algorithm.

Cytoskeletal filament	**Conditions and Perturbations**	**Sampling rate (sec)**	**Pixel size (µm)**	**Reference**
Opposite microtubule bundles in mitotic spindle extracts	*1. Wild type (control) & 2. AMP-PNP, 5µM*	10	67	(*19*)
	3. S-trityl-L-cysteine, 100mM &	5	67	(*17*)
	4. Monastrol, 0.5–1 mg/ml			
	5. Needle skewering	5	129	(*23*)
Contractile actin meshworks in migrating epithelial cells and neurons	*6. Rac1 activation (data not shown) (Ptk1 cells)*	5	67	(*35*)
	7. Wild type (Ptk1 cells)	10	67	(*25*)
	8. Wild type & 9. Blebbistatin, 70 µM (Growth cones in primary cultures of Aplysia bag cell neurons)	10 & 5	133	(*26*)
	10. Tm2 over-expression & 11. Tm4 over-expression (Ptk1 cells)	10	67	*Prepared for this paper by Dr. Bacconi*

Table 1: Data description. This paper presents additional computational analysis of previously analyzed and published image datasets in six manuscripts and two new conditions, two tropomyosin isoforms over-expression, prepared specifically for this

publication. IFTA adds a new level of insight in addition to the already available information about speckle flows delivered by earlier tracking methods (*3-5*).

5.2. Image analysis

All image analysis programs for detection and tracking of speckles and graphical representation of the results were developed in MATLAB (Mathworks, MA) and C/C++. The speckle detection method ClusterTrack used is described and validated in (*36*), the tracking method IFTA is described and validated in (*2*). The computer code is available for download at: https://www.github.com/amatov/ InstantaneousFlowTracker. The CPLEX optimizer requires an ILOG license from IBM.

5.3. Cell culture

Kangaroo rat kidney epithelial PtK1 cells were cultured as described previously (*35*).

5.4. Development of tropomyosin cell lines

5.4.1. Molecular cloning

Human Tm2 and Tm4 sequences, derived from NCBI GenBank database, were cloned from MDA-MB231 receptor triple-negative breast cancer cells. Total RNA was isolated by RNeasy Mini Kit (Qiagen), retrotranscribed and the specific tropomyosin sequences were amplified by PCR. The long (Tm2) and short (Tm4) human isoforms were ligated into the pIRES2-AcGFP1 expression vector (Clontech).

5.4.2. Ptk1 cells transfection

PtK1 cells were transfected by nucleofector technology (Lonza) with recombinant pIRES2-AcGFP1 vectors expressing Tm2 and Tm4 respectively.

5.5. Microscopy

Imaging was performed with a spinning disk confocal with cool snap HQ2 camera on a Nikon 3200 with Perfect Focus and 100X objective. Images were acquired every 10 seconds for at least 10 minutes.

5.6. FSM of Ptk1 cells

X-rhodamine–conjugated actin was prepared as described previously (*37*) and microinjected into cells at 1 mg/ml.

6. ACKNOWLEDGEMENTS

The authors are grateful to Stephanie Gupton, Dylan Burnette, Aaron Groen, Gaudenz Danuser, Torsten Wittmann, and Pascal Vallotton for sharing raw image datasets from published papers and their feedback regarding the shortcomings of the previous analysis methods.

7. SUPPLEMENTARY MATERIALS

Video 1 – AMPPNP-Treated Spindle Exhibiting No Microtubule Flux.

Video 2 – Monastrol-Treated Monopole Spindle Exhibiting Inward Microtubule Flux.

Video 3 – Growth Cone Exhibiting a Slight Contraction in the Base of the Cone of the Two Entangled Actin Flows.

Video 4 – Four Directional Actin Flux in a Cell with Over-expression of Tm2.

A Three-Panel Movie: The Left Panel Displays the Whole Cell, the Middle Panel Displays a Zoomed-in Area in Which the Vectors from the Tracking are Showed, the Left Panel Displays a Dynamic Overlay of the Original Images with the Four Overlapped Flow Fields. Yellow Arrows Show the Retrograde Flow Field Vectors, Green Arrows Show the Anterograde Flow Field Vectors, Black Arrows Show the Vectors of the Upward Flow Field Vectors, and Red Arrows Show the Downward Flow Field Vectors.

8. REFERENCES

1. G. Yang *et al.*, Architectural Dynamics of the Meiotic Spindle Revealed by Single-Fluorophore Imaging. *Nat Cell Biol* **9**, 1233 - 1242 (2007).

2. A. Matov, M. M. Edvall, G. Yang, G. Danuser, Optimal-flow minimum-cost correspondence assignment in particle flow tracking. *Computer Vision and Image Understanding* **115**, 531-540 (2011).

3. A. Ponti *et al.*, Periodic patterns of actin turnover in lamellipodia and lamellae of migrating epithelial cells analyzed by Quantitative Fluorescent Speckle Microscopy. *Biophys J* **89**, 3456-3469 (2005).

4. G. Yang, A. Matov, G. Danuser, *IEEE Conference on Computer Vision and Pattern Recognition (CVPR)*, June 20: 138-146 (2005).

5. L. Ji, G. Danuser, Tracking quasi-stationary flow of weak fluorescent signals by adaptive multi-frame correlation. *J Microscopy* **220**, 150-167 (2005).

6. T. M. Kapoor, T. J. Mitchison, Eg5 is static in bipolar spindles relative to tubulin: evidence for a static spindle matrix. *The Journal of Cell Biology* **154**, 1125-1134 (2001).

7. L. C. Kapitein *et al.*, Microtubule cross-linking triggers the directional motility of kinesin-5. *The Journal of Cell Biology* **182**, 421-428 (2008).

8. C. M. Waterman-Storer, A. Desai, J. C. Bulinski, E. D. Salmon, Fluorescent speckle microscopy, a method to visualize the dynamics of protein assemblies in living cells. *Current Biology* **8**, 1227-1230 (1998).

9. P. Vallotton, A. Ponti, C. M. Waterman-Storer, E. D. Salmon, G. Danuser, Recovery, visualization, and analysis of actin and tubulin polymer flow in live cells: A Fluorescence Speckle Microscopy Study. *Biophys J* **85**, 1289 - 1306 (2003).

10. A. Desai, A. Murray, T. J. Mitchison, C. Walczak, The use of Xenopus egg extracts to study mitotic spindle assembly and function in vitro. *Methods Cell Biol* **61**, 385 - 412 (1999).

11. G. Yang, L. A. Cameron, P. Maddox, E. D. Salmon, G. Danuser, Regional Variation of Microtubule Flux Reveals Microtubule Organization in the Metaphase Meiotic Spindle. *The Journal of Cell Biology* **182**, 631-639 (2008).

12. K. E. Sawin, T. J. Mitchison, Poleward Microtubule Flux in Mitotic Spindles Assembled In Vitro. *The Journal of Cell Biology* **112**, 941-954 (1991).

13. Z. E. Perlman *et al.*, Multidimensional Drug Profiling By Automated Microscopy. *Science* **306**, 1194-1198 (2004).

14. K. E. Sawin, T. J. Mitchison, Mitotic Spindle Assembly by 2 Different Pathways Invitro. *The Journal of Cell Biology* **112**, 925-940 (1991).

15. J. C. Gatlin *et al.*, Spindle Fusion Requires Dynein-Mediated Sliding of Oppositely Oriented Microtubules. *Current Biology* **19**, 287-296 (2009).

16. T. J. Mitchison *et al.*, Bipolarization and Poleward Flux Correlate during Xenopus Extract Spindle Assembly. *Mol Biol Cell* **15**, 5603-5615 (2004).

17. D. T. Miyamoto, Z. E. Perlman, K. S. Burbank, A. C. Groen, T. J. Mitchison, The kinesin Eg5 drives poleward microtubule flux in Xenopus laevis egg extract spindles. *The Journal of Cell Biology* **167**, 813-818 (2004).

18. G. C. Rogers, S. L. Rogers, D. J. Sharp, Spindle microtubules in flux. *Journal of Cell Science* **118**, 1105-1116 (2005).

19. L. A. Cameron *et al.*, Kinesin 5-independent poleward flux of kinetochore microtubules in PtK1 cells. *The Journal of Cell Biology* **173**, 173-179 (2006).

20. J. Gaetz, T. M. Kapoor, Dynein/dynactin regulate metaphase spindle length by targeting depolymerizing activities to spindle poles. *The Journal of Cell Biology* **166**, 465-471 (2004).

21. J. Brugués, V. Nuzzo, E. Mazur, D. J. Needleman, Nucleation and transport organize microtubules in metaphase spindles. *Cell* **149** 554-564 (2012).

22. B. R. Houghtaling, G. Yang, A. Matov, G. Danuser, T. M. Kapoor, Op18 Reveals the Contribution of Non-Kinetochore Microtubules to the Dynamic Organization of the Vertebrate Meiotic Spindle. *Proc Natl Acad Sci U S A* **106**, 15338-15343 (2009).

23. J. C. Gatlin, A. Matov, G. Danuser, T. J. Mitchison, E. D. Salmon, Directly probing the mechanical properties of the spindle and its matrix. *The Journal of Cell Biology* **188**, 481-489 (2010).

24. Y. Shimamoto, T. M. Kapoor, Microneedle-based analysis of the micromechanics of the metaphase spindle assembled in Xenopus laevis egg extracts. *Nature Protocols* **7**, 959-969 (2012).

25. S. L. Gupton, C. M. Waterman-Storer, Spatiotemporal feedback between actomyosin and focal-adhesion systems optimizes rapid cell migration. *Cell* **125**, 1361-1374 (2006).

26. D. T. Burnette, A. W. Schaefer, L. Ji, G. Danuser, P. Forscher, Filopodial Actin Bundles are not Necessary for Microtubule Advance into the Peripheral Domain of Aplysia Neuronal Growth Cones. *Nat Cell Biol* **9**, 1360 - 1369 (2007).

27. D. T. Burnette *et al.*, Myosin II activity facilitates microtubule bundling in the neuronal growth cone neck. *Dev Cell* **15**, 163-169 (2008).

28. J. G. Lees, C. T. Bach, G. M. O'Neill, Interior decoration: tropomyosin in actin dynamics and cell migration. *Cell Adh Migr* **5**, 181-186 (2011).

29. C. L. Wang, L. M. Coluccio, New insights into the regulation of the actin cytoskeleton by tropomyosin. *Int Rev Cell Mol Biol* **281**, 91-128 (2010).

30. S. L. Gupton *et al.*, Cell migration without a lamellipodium: translation of actin dynamics into cell movement mediated by tropomyosin. *The Journal of Cell Biology* **168**, 619-631 (2005).

31. A. Ponti, M. Machacek, S. L. Gupton, C. M. Waterman-Storer, G. Danuser, Two distinct actin networks drive the protrusion of migrating cells. *Science* **305**, 1782 - 1786 (2004).

32. M. A. T. Figueiredo, A. K. Jain, Unsupervised learning of finite mixture models. *IEEE Trans. Pattern Analysis and Machine Inteligence (PAMI)* **24**, 381-396 (2002).

33. P. W. Gunning, G. Schevzov, A. J. Kee, E. C. Hardeman, Tropomyosin isoforms: divining rods for actin cytoskeleton function. *Trends in Cell biology* **15**, 333-341 (2005).

34. P. Kumar *et al.*, GSK3β phosphorylation modulates CLASP–microtubule association and lamella microtubule attachment. *The Journal of Cell Biology* **184**, 895-908 (2009).

35. T. Wittmann, G. M. Bokoch, C. M. Waterman-Storer, Regulation of leading edge microtubule and actin dynamics downstream of Rac1. *The Journal of Cell Biology* **161**, 845-851 (2003).

36. A. Matov *et al.*, Analysis of microtubule dynamic instability using a plus end growth marker. *Nature Methods.* **7**, 761-768 (2010).

37. C. M. Waterman-Storer, *Current Protocols in Cell Biology*, J. S. Bonifacino, M. Dasso, J. B. Harford, J. Lippincott-Schwartz, K. M. Yamada, Eds. (Wiley, New York) (2002).